Numerical and experimental studies of collection efficiency of an ion electrostatic collector for a mini-volume electrical PM detector

Panich Intra [a, *], Artit Yawootti [a], Phadungsak Rattanadecho [b]

[a] Research Unit of Electrostatic Applications in Energy and Environment, College of Integrated Science and Technology, Rajamangala University of Technology Lanna, Chiang Mai 50220, Thailand
[b] Center of Excellence in Electromagnetic Energy Utilization in Engineering, Department of Mechanical Engineering, Faculty of Engineering, Thammasat University, Pathum Thani 12121, Thailand

ARTICLE INFO

ABSTRACT

The experimental efficiency was numerically and experimentally studied for collecting negative and positive ions in a coaxial cylindrical electrostatic collector for a mini-volume electrical PM detector. The commercial computational fluid dynamics software package COMSOL Multiphysics™ was used to predict the behaviors of the flow and electric fields as well as the particle trajectories in the collecting zone of the ion collector. In the experiment, the ions were generated by a corona-needle ionizer with concentrations greater than 10^{13} ions/m^3, the positively and negatively applied voltages at the inner electrode ranged from 0 to 45 V and the ion flow rates ranged from 1 to 5 L/min. For these ion flow rates, 1—5 L/min, the ion precipitates due to space charge and diffusion effects ranged from 92 to 97 % for positive ions and 91 −97 % for negative ions. The total collection efficiency of the collector increased to 100% at collection voltages larger than 5, 20 and 40 V respectively for the ion flow rates of 1, 3 and 5 L/min for both positive and negative ions. Numerical calculation results of the ion trajectory in the collecting zone of the collector; showed good agreement with the experimental results of the total collection efficiency and can be used to support the bettering of designing in order to refine an ion collector after the charger or ionizer in a mini-volume electrical aerosol detector. Finally, this shows that this ion collector was proven to be particularly useful as an electrostatic collector for positive and negative ions after the charger or ionizer in a mini-volume electrical aerosol detector.

© 2014 Elsevier B.V. All rights reserved.

Introduction

Measurement of concentration of the particulate matter (PM), any solid or liquid material suspended in air with aerodynamic diameter in the range of 1 nm−100 μm, have become an important topic in atmospheric pollution monitoring and source characterization. In recent years, considerable interest has been shown to micron-sized aerosol particles, defined as suspended aerosol particles with aerodynamic diameter lower than 2.5 μm, for two main reasons. First, such particles have been associated with adverse health effects in areas of high concentrations, and second, aerosols are believed to have a significant influence on atmospheric quality, climate at a local and global scale and processes in various industries such as food, pharmaceutical and medical, electronic and semiconductor industries [1]. PM detectors have been developed to monitor indoor and outdoor aerosols for pollution and process control industry for this purpose.

A widely used instrument capable of detecting and measuring PM is an electrical PM detector. A typical PM detector consists of an aerosol charger, an ion collector, and an aerosol electrometer. In the PM detector, aerosols are directed into the aerosol charger to charge the aerosol particles by ion-particle collisions via the diffusion charging and field charging mechanisms. The charged aerosol then passes through an ion collector to remove excess ions and moves on to a highly sensitive aerosol electrometer for charge measurement [2,3]. Generally, an ion collector is one of the most important parts of the electrical PM detector because it can prevent contamination of the signal current to be measured by free ions potentially reaching the electrometer [4]. The ion collector typically uses the principle of electrostatic precipitation and has a geometrical configuration similar to the coaxial cylindrical electrostatic precipitator. It consists of an inner electrode placed along the axis of an outer electrode. For generating an electrostatic field inside the

* Corresponding author.
  E-mail address: panich_intra@yahoo.com (P. Intra).

collector a DC voltage is applied to the inner electrode, while the outer electrode is grounded. When ions are introduced into the collector, the electrostatic force drives them toward the outer electrode where they deposit on the inner surface of the electrode. The design and performance evaluation of the ion collector has received little attention in the literature [5–12]. Higher applied voltages (10–150 V) and flow rates (5–15 L/min) were theoretically and experimentally studied by numerous works [5–7,12]. However, a mini-volume electrical PM detector commonly has been operated at volumetric aerosol flow rates lower than 5 L/min and therefore needed a compactable system for a field test and measurement. Therefore, an ion electrostatic collector needs to be designed and numerically and experimentally evaluated for the efficiency of collecting both negative and positive ions at ion flow rates smaller than 5 L/min and collection voltages lower than 50 V. The geometry, dimension and size of the ion collector would have influenced to the complexity and expense of the ion collector and then to keep it cost effective.

This paper presents the work of designing and evaluating an electrostatic collector that collects highly electrical mobile positive and negative ions after the charger or ionizer of the mini-volume electrical PM detector. Its collection characteristics were experimentally determined at applied voltages at the inner electrode between 0 and 45 V, ion flow rates between 1 and 5 L/min, and an operating pressure of about 1.01×10^5 Pa. The ions precipitates due to space charge and diffusion effects were evaluated. Also, a commercial computational fluid dynamics software package COMSOL Multiphysics™ was used to predict the behavior of the flow and electric fields as well as the ion and particle trajectories in the collecting zone of the ion collector.

Description of an ion electrostatic collector

Fig. 1 shows the schematic diagram of the ion collector used in this study. The geometrical configuration is similar to that in the ion collector used by Intra and Tippayawong [4]. However, the differences between the previous and the present were as follows; (i) short column collector was used to reduce diffusion and space charge losses of the aerosol particles inside the collector; and (ii) it is a low complexity and inexpensive system. This ion collector
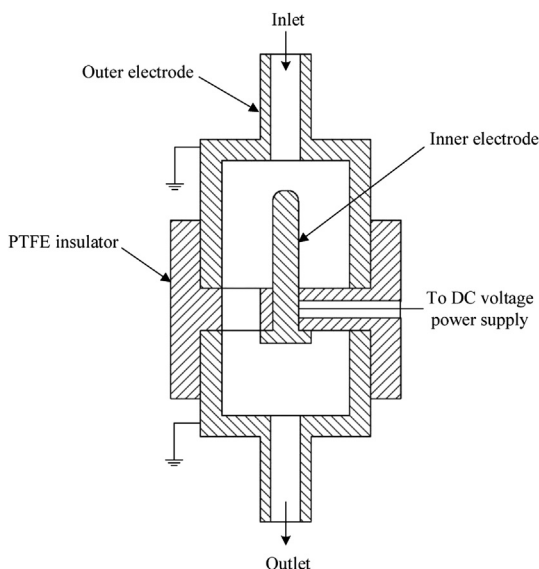

Fig. 1. Schematic diagram of the ion collector.

consisted of a coaxial cylindrical electrode placed along the axis of a metallic cylindrical tube and divided into three sections. The first and third sections (from the upper part to the lower part in the diagram) were made of a stainless steel tube and the second a polytetrafluoroethylene (PTFE) tube. The PTFE tube is an electrical insulator and it was placed between the two stainless steel tubes, the hole through which the ion flow, and served to hold the inner electrode coaxial with the outer electrode. The inner electrode could be screwed into the PTFE insulator to connect a DC voltage supply. The outer electrode was 15 mm in an inner diameter and 15 mm in length, and the inner electrode was made of a stainless steel with an outer diameter of 3 mm and a length of 11.5 mm. The inner and outer electrodes were polished to an extremely fine surface finish, and the head of the inner electrode was rounded to a 1.25 mm radius to ensure the uniform flow and electric fields inside the collector. The DC voltage supply applied to the inner electrode, was typically in the range between 0 and 45 V, whereas the outer metallic electrode was grounded.

Mathematical model and numerical simulation

It was well known that the fluid flow, the electric field distribution, and the ion transport behavior within the ion collector has been reported in our previous work by Intra and Tippayawong [12] to have important factors influencing on its collection efficiency depending on the arrangement of major geometrical features inside an ion collector. It is difficult to carry out detailed and reliable measurement of the fluid flow, the electric field distribution, and the ion and particle transport inside an ion collector as the geometry is very complex. Numerical simulation provides an alternative method, which is reliable and less expensive to study the fluid flow, the electric field distribution, and the ion transport behavior inside the ion collector. The mathematical model and numerical simulation used in this study were as follows:

Governing equations

To the accurate model of the ion collector, three partial differential equations (PDE) were selected and coupled in the commercial software package COMSOL Multiphysics™, namely, the Poisson's and Navier–Stokes equations as well as the Khan and Richardson force [13]. The governing equations are given by:

Governing equations for the electrostatics

For electrostatic field modeling, electrostatic fields are generated by a combination of stationary charges and applied potentials. Electrostatics is governed by Gauss's Law, which states that the net electric flux passing through a closed surface is equal to the net charge enclosed by that surface. Therefore, the electric potential V is governed by Poisson's equation and given by.

$$\nabla^2 V = \frac{\rho_v}{\varepsilon_0} \tag{1}$$

where ρ_v is the space charge density and ε_0 is the dielectric permittivity of free space. Since most ion collector application involve aerosol concentration lower than 10^6 particles/cm3, and with low particle charge level, the space-charge effect on the electric field is neglected ($\rho_v = 0$). The electric potential is derived from the electric field intensity E and it is given by

$$E = -\nabla V \tag{2}$$

Governing equations for the air flow

The air flow inside the collector can be assumed to be steady, incompressible and laminar. Based on the principle of momentum conservation, the air flow has been modeled by using COMSOL software incorporating a laminar flow, using the Reynolds averaged Navier–Stokes equations for incompressible gas in this work. The mean velocity, field and pressure and determined using the $\kappa - \varepsilon$ parameters as defined in the software [13].

$$\rho_{gas}\left(u\cdot\nabla\right)u = -\nabla p + \mu_{gas}\nabla^2 u + F \tag{3}$$

$$\nabla\cdot u = 0 \tag{4}$$

where u is the air velocity, μ_{gas} is the dynamic viscosity of the air, ρ_{gas} is the air density, p is the pressure and F is the force field. The pressure at the outlet is the atmospheric pressure (P_0) and no viscous stress is used:

$$\eta(\nabla u + (\nabla u)^T n = 0 \text{ and } P = P_0 \tag{5}$$

where T is the transposed matrix. The no slip boundary condition was considered for the wall boundary conditions.

Governing equations for the particle trajectories

There are four forces acting on each particle which is given by gravity force: $\vec{F}_g = \rho_p g 2\pi a^3/3\vec{z}$, archimedes force: $\vec{F}_a = -\rho_{gas} g 2\pi a^3/3\vec{z}$, electrostatic force: $\vec{F}_e = q_{max}E(r)\cdot\vec{r}$ and drag force: $\vec{F}_d$; where a is the particle radius, ρ_p is the particle density, q_{max} is the maximum number of charge per particle, and g is the gravity constant. The drag force is modeled by the Khan and Richardson force which is calculated by the COMSOL software [13].

The following equation describes the total force that a fluid exerts on an immersed spherical particle:
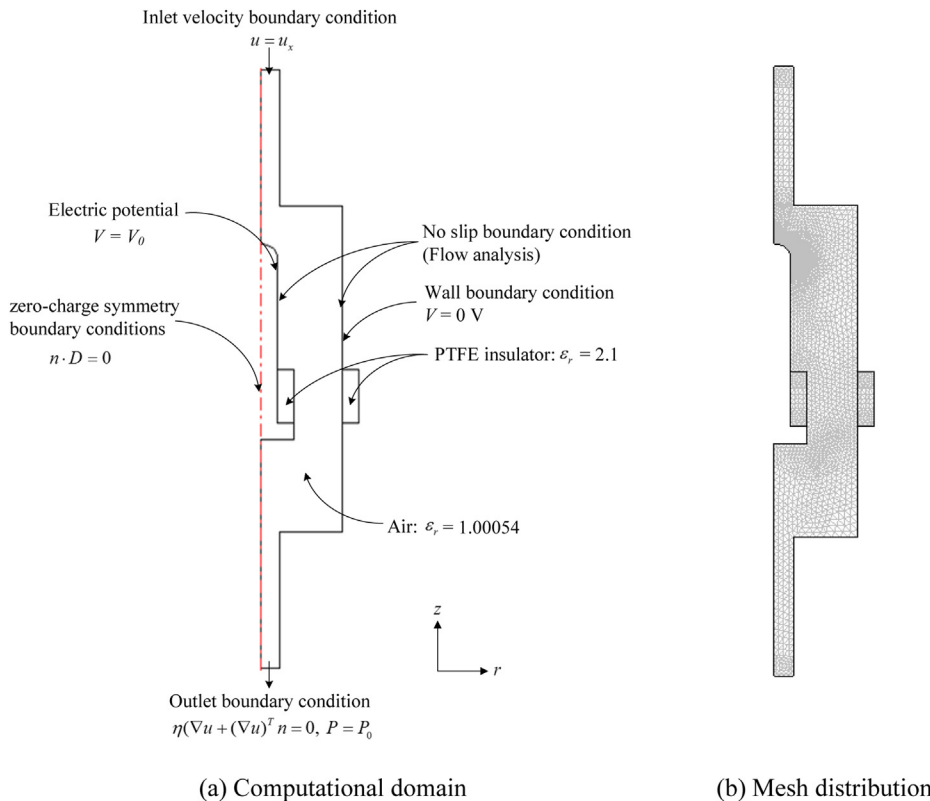
$$\vec{F}_d = \pi a^2 \rho_{gas}\left(\vec{u} - \vec{u}_p\right)\left[1.84(Re_p)^{-0.31} + 0.293(Re_p)^{-0.06}\right]^{3.45} \tag{6}$$

$$Re_p = \frac{2a\rho_{gas}\left(\vec{u} - \vec{u}_p\right)}{\mu} \tag{7}$$

where Re_p is the particle Reynolds number, $\vec{u}$ is the velocity field of the gas and $\vec{u}_p$ is the particle velocity.

Computational domain and boundary conditions

Computational domain for flow and electric fields of the ion collector is shown in Fig. 2 (a). For the collection zone, the Poisson's Equation (1) and the electric potential Equation (2) were solved using the electrostatic module and the PDE module to obtain a steady state field and charge density distribution. Dirichlet boundary conditions were used in the PDE module, with an initial space charge density on the inner electrode boundary along with zero ion concentration on the outer electrode. In the electrostatic module, a ground (0 V) has been implemented on the outer electrode and the electric potential on the inner electrode (ranging from 0 to 45 V). The zero-charge symmetry boundary condition was applied to the boundaries without walls, and is given by $n\cdot D = 0$ where n is the outward normal from medium and D is the electric flux density. The flow inside the ion collector could be assumed to be steady, incompressible and laminar. Based on the principle of momentum conservation, the incompressible Navier–Stokes

Inlet velocity boundary condition
$u = u_x$

Electric potential
$V = V_0$

zero-charge symmetry
boundary conditions
$n\cdot D = 0$

No slip boundary condition
(Flow analysis)

Wall boundary condition
$V = 0$ V

PTFE insulator: $\varepsilon_r = 2.1$

Air: $\varepsilon_r = 1.00054$

Outlet boundary condition
$\eta(\nabla u + (\nabla u)^T n = 0, P = P_0$

(a) Computational domain   (b) Mesh distribution

Fig. 2. Computational domain and mesh distribution for flow and electric fields of the ion collector.

Table 1
Operating condition values of the experiments.

| Parameter and operating conditions	Values
Diameter of inner electrode (mm)	3
Diameter of outer electrode (mm)	15
Length of collector (mm)	15
Inner electrode voltage (V)	0 − 45
Ion flow rate (L/min)	1, 3, 5
Operating temperature (K)	294
Operating pressure (atm)	1
Polarity of ions	Positive and negative

equations (N−S equation) can be applied in this case. A wall boundary condition has been implemented on both electrodes, i.e., a pressure of 1.01×10^5 Pa on the outlet and a normal velocity field in the inlet. The operating gas was ambient air (density was 1.19 kg/m^3, viscosity was 1.79×10^{-5} kg/m/s, and the relative permittivity constant was 1.00054). The PTFE insulator permittivity constant was 2.1.

Fig. 2 (b) shows the mesh distribution for the flow and electric fields of the ion collector. The considered problem was discretized with the finite element method (FEM), and utilizing triangular elements for the axis-symmetric two-dimensional model. The mesh was automatically generated by COMSOL and was refined in critical regions such as the inner electrode head and between outer electrode and insulators. This convergence test results in number of triangular elements of approximately 4608. The computations were carried out on a desktop running a 64 bit OS Windows 7. Core i5 processors (each 2.40 GHz) and 4 GB of RAM are allowed for solving the model within the approximation of the 3 min of computation time. The values of various parameters, which have been used in this study, are given in Table 1. After solving the fluid dynamic equations together with the electrostatic parameters, it is possible to trace the particulate trajectories.

Experimental setup

In order to use the numerical simulation to analyze the fluid flow, electric field distribution, and ion and particle transports behavior within the ion collector, it is necessary to evaluate the simulation. Experimental study has been carried out for evaluating the numerical simulation. Fig. 3 shows the experimental setup for investigating the collection efficiency of the ion collector. It consisted of an ionizer, a DC voltage power supply, a Faraday cup, an electrometer, a high efficiency particulate-free air (HEPA) filter, and a flow system. A high concentration of ions was generated by corona discharge with the corona-needle ionizer developed by Intra and Tippayawong [14,15] as shown in Fig. 4. The ion concentration at the ionizer outlet was measured by the Faraday cup electrometer. Fig. 5 shows the number concentration of positive and negative ions as a function of the corona voltage at the ionizer outlet, usually greater than 10^{13} ions/m^3, at operating flow rate between 1 and 5 L/min and the corona voltage between 2.3 and 3.4 kV [15]. As shown in Fig. 5, the ion concentration at the ionizer outlet was found to be relatively high with the same corona voltage at higher air flow rates, because the free ions can be more easily drawn off the ionizer by faster flowing air [14–16].

In this experimental study, the ion collector was connected directly to the ionizer outlet via a very short connecting pipe. The connecting pipe is made of a stainless steel, 3.5 mm in an inner diameter and a length of 10 mm. The airflow was regulated and controlled by a mass flow meter and controller (Dwyer model GFC-1111) with a vacuum pump located at the end of the experimental equipment train. The mass flows were typically in the range between 1 and 5 L/min. A silica gel drying chamber was used to remove any remaining water from an air sample. Dried air samples were filtered through a Pall HEPA capsule filter (model 12144) and were then drawn into the ionizer. An adjustable commercial DC high voltage power supply (Leybold Didactic model 521721) was used to maintain the corona voltage difference in the ionizer,
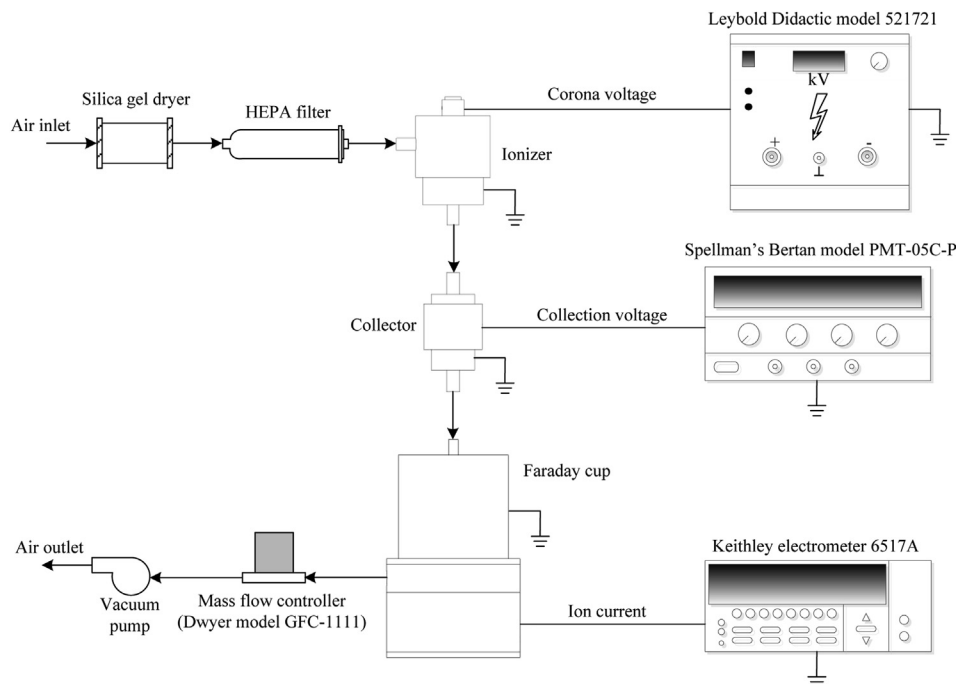
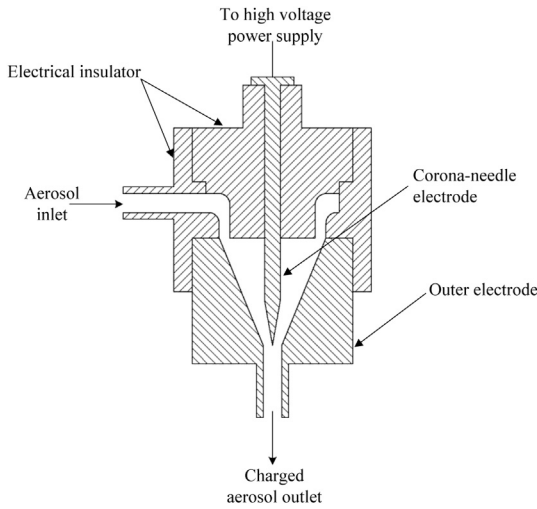**Fig. 3.** Experimental setup for investigating the efficiency of the ion collector.

Fig. 4. Schematic diagram of the corona-needle ionizer.

generally 3.0 and 2.7 kV for positive and negative coronas, respectively. The ions produced inside the ionizer then entered the ion collector. A second adjustable commercial DC voltage power supply, Bertan model PMT-05C–P, was used to maintain the positive and negative voltages difference in the collector, generally in the range between 0 and 45 V.

After the ion collector, the air sample with ions entered the Faraday cup as shown in Fig. 6 [16], where the ion current was measured with Keithley 6517A electrometer. In order to eliminate the leakage currents, the collecting electrode (filter holder) of the Faraday cup was connected to the electrometer input that had been carefully shielded against external fields with the low-noise triaxial connection cables, Keithley 237-ALG-2. The Keithley 237-ALG-2 has an insulation resistance of 10^{15} Ω, center conductor to shield, and contact resistance of <0.5 Ω. As shown in Fig. 5, it can be shown that the ion number concentration at the ionizer outlet corresponded to the operating air flow rate. Thus, the number concentration of positive and negative ions at the ionizer outlet, N_p and N_n, could be calculated from the expression by Lehtimaki [5]:

$$N_p = I_p/eQ \qquad (8)$$

$$N_n = I_n/eQ \qquad (9)$$

where I_p and I_n are the currents of the positive and negative ions from the Faraday cup, e is the value of the elementary charge on an electron (1.60×10^{-19} C) [1], and Q is the volume flow rate of ions. Therefore, the collection efficiency η, was calculated by

$$\eta = 1 - \frac{N_{\text{outlet}}}{N_{\text{inlet}}} \qquad (10)$$

where N_{outlet} and N_{inlet} are number concentration of ions at the outlet and inlet. Table 1 shows the values for the operating condition values of the experiment.

Results and discussion

Fig. 7 (a) shows the numerical calculation results of the gas flow field, namely the streamline and velocity field, inside the ion collector. In this calculation, the air flow velocity at the ion collector inlet was about 7.073 m/s or the air flow rate was about 3 L/min. It is noted that the domain is represented at the symmetry plane. It was showed that the flow field has the highest velocity at the inlet and outlet of the ion collector. The flow velocity generally peaks at the axis and decreases towards the wall of the outer electrode. Uniformity of the velocity field was presented in the collecting zone of the collector. Fig. 7 (b) shows the characteristics of the electric field inside the ion collector when 40 V was applied at the inner electrode. It was observed that the electric field was distributed with the highest strength near the head and end of inner electrode whereas electric field decreased in magnitude from the edge of the inner electrode to the outer electrode of the collector. It was also found that the holder insulator of the inner electrode could be used to change the distribution and uniformity of the electric field in the collecting zone as shown in Fig. 7 (b).

It is possible to trace the ions and particles trajectories with COMSOL Multi-physics. Fig. 8 shows the ion trajectories inside the ion collector at different operating collecting voltage of 10–40 V and air flow rate of about 3 L/min or air flow velocity of about 7.073 m/s. In this simulation, the ionic mass and radius was assumed about 3×10^{-18} g and 30×10^{-12} m, respectively [17]. It has been observed that the collection efficiency of ions increases with respect to the applied collecting voltage. It was also found that
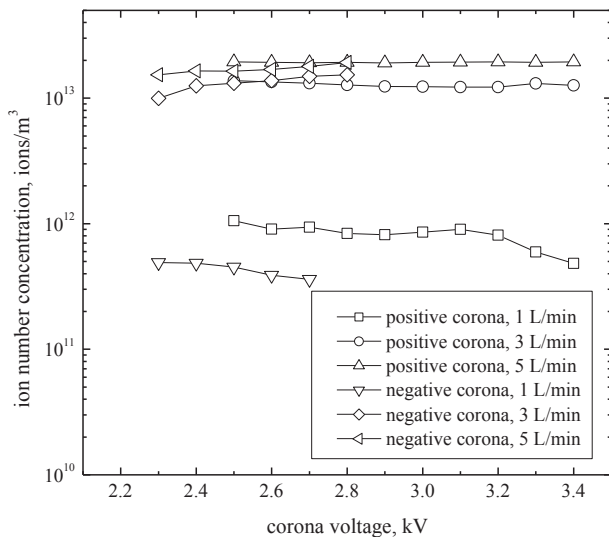

Fig. 5. Variation in ion number concentration with corona voltage at the corona-needle ionizer outlet.
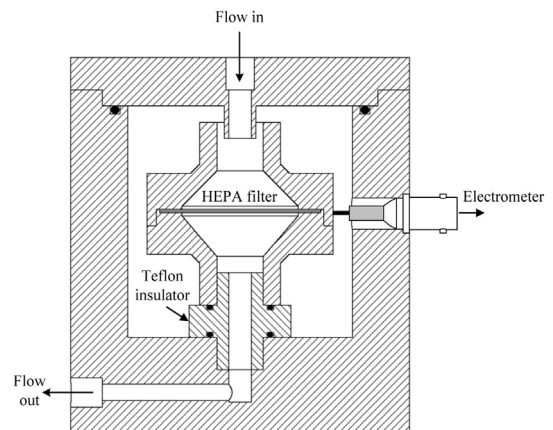

Fig. 6. Schematic diagram of the Faraday cup.
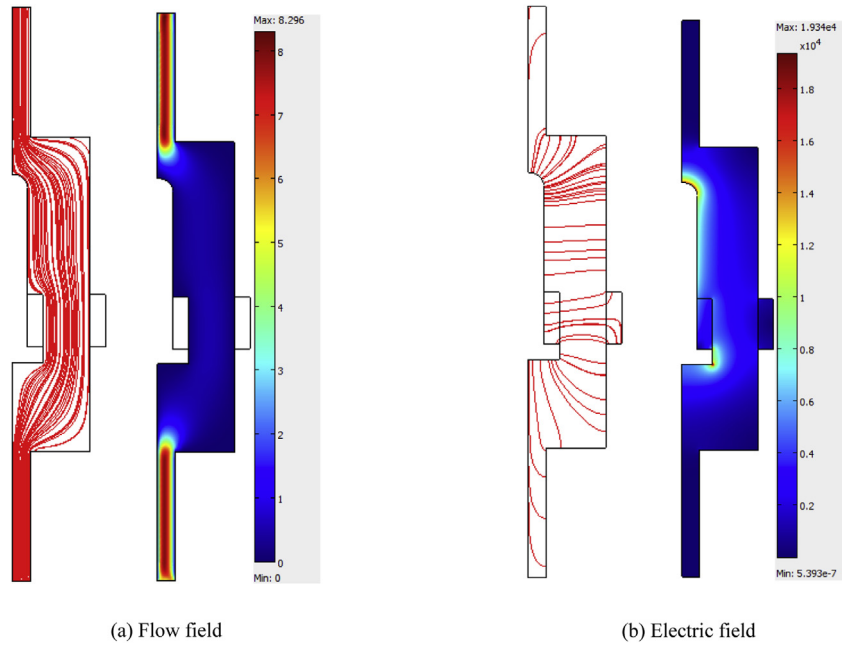
(a) Flow field   (b) Electric field

Fig. 7. Flow and electric fields inside the ion collector.

all ions were collected on the outer electrode of the ion collector at a collecting voltage larger than 20 V.

In case of particle trajectories, Fig. 9 shows the particle trajectories inside the ion collector at different particle diameter of 0.1, 1.0, 2.5 and 10 μm and collecting voltage of 40 V with air flow velocity of 8.666 m/s. The particle mass was about 5.22×10^{-19}, 5.15×10^{-16}, 5.0×10^{-15} and 5.17×10^{-13} g corresponding to the particle diameter of 0.1, 1.0, 2.5 and 10 μm, respectively [1]. In this study, the mean of charge per particle was approximated by White's charging equation for the field and diffusion charging [18]. It should be noted that the field charging was dominant for particles larger than 0.5 μm, and for smaller particles smaller than

0.2 μm, thermal diffusion became dominant, and therefore diffusion charging became important [1]. In case of the particle diameter of 1.0, 2.5 and 10 μm, the mean charge per particle were usually based on combined diffusion and field charging where particle charge is the sum of the contributions from field and diffusion charge [19]. Therefore, the mean of charge per particle was about 5.6, 162, 1000 and 16,540 electrons for the particle diameter of 0.1, 1.0, 2.5 and 10 μm, at the N_it product of 1.28×10^{13} ions/m³ s, the corona voltage of 3.4 kV, the electric field strength of 2×10^6 V/m, and the dielectric constant of 3.0, respectively. It was well known that the collection efficiency of charged particles mainly depended on the electric field strength inside the collector and the particle
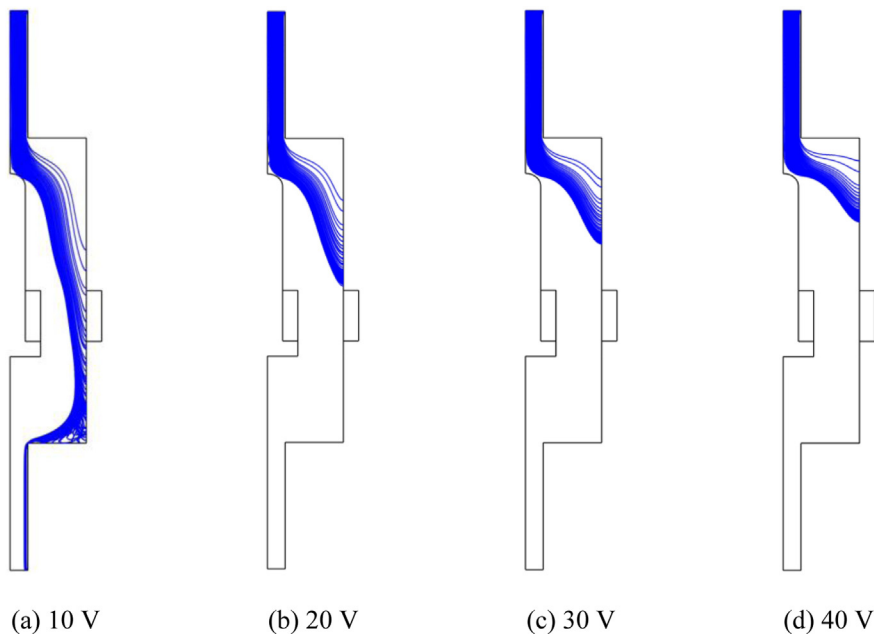

(a) 10 V   (b) 20 V   (c) 30 V   (d) 40 V

Fig. 8. Ion trajectories inside the ion collector at different operating collecting voltage.

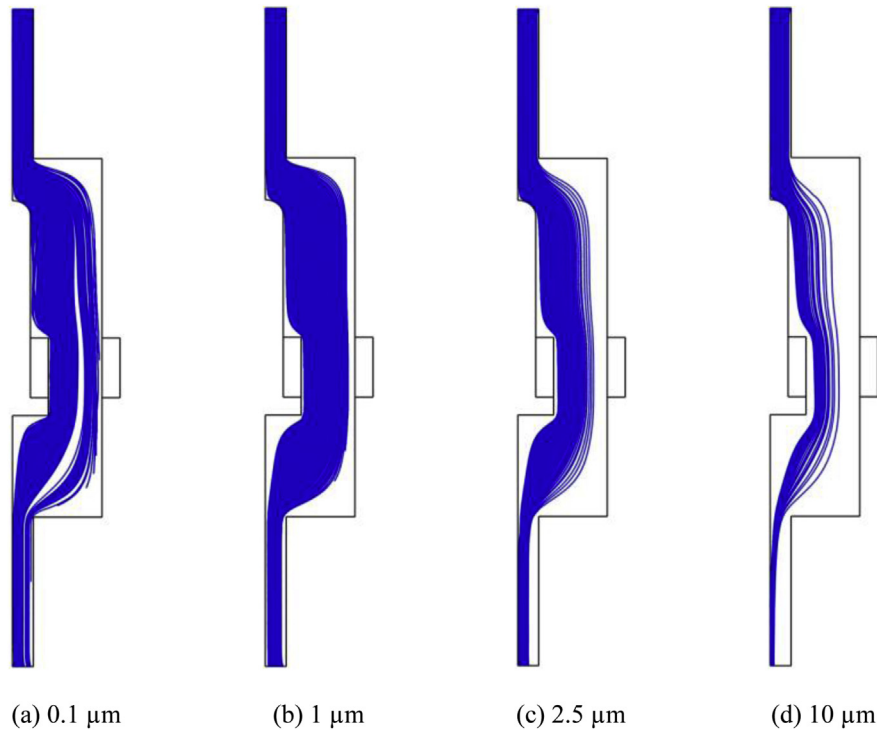(a) 0.1 μm　　　(b) 1 μm　　　(c) 2.5 μm　　　(d) 10 μm

Fig. 9. Particle trajectories inside the ion collector at different particle diameter.

electrical mobility as a function of a particle diameter. Large particle diameter has higher mean charge than small particle diameter, therefore, electrostatic force applied on the particle increased with respect to the mean charge per particle as a function of its diameter. An increase in electrostatic force on the charged particles produced an increase in the collection efficiency of the charged particles of the ion collector. It has been shown in Fig. 9, and it can be observed that all charged particles of 0.1, 1.0, 2.5 and 10 μm can pass through the collector smoothly without precipitate on the outer electrode of the ion collector. It should be noted these calculation results can be used to support the bettering of further modify and refinement of the ion collector and also to understand the mechanisms of the ion transport and collecting inside the ion collector.

Fig. 10 shows the variation of the ion concentration of the ionizer and collector outlets with ion flow rate. At higher ion flow rates, the ion number concentration was high. The magnitude of the ion number concentration at the ionizer outlet was much larger than at the ion collector outlet. It was expected that ions partially would be lost by electrostatic deposition inside the ion collector due to Brownian diffusion, electrostatic dispersion
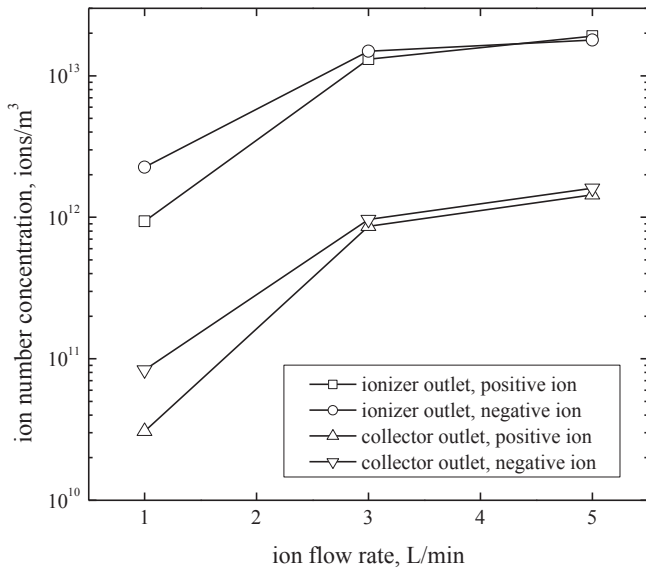

Fig. 10. Variation of ion concentration of ionizer and collector outlets with ion flow rate.
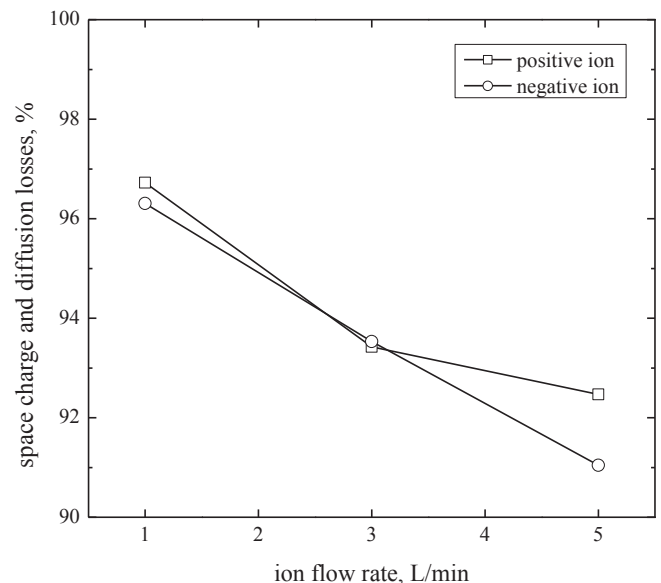

Fig. 11. Space charge and diffusion losses of ions as a function of ion flow rate.

(space charge) and an external electric field. With ion concentrations above 10^{13} ions/m^3, ions may partially deposit onto the inner and outer electrodes of the ion collector by space charge effects in the absence of any applied voltage on the inner electrode. As shown in Fig. 10, the ion number concentration at the ionizer outlet had a range from 9.38×10^{11} to 1.91×10^{13} ions/m^3, and 2.26×10^{12} to 1.79×10^{13} ions/m^3 for positive and negative corona voltages, respectively. The number concentration of both positive and negative ions at the collector outlet was in the range from 3.07×10^{10} to 1.44×10^{12} ions/m^3, and 8.35×10^{10} to 1.60×10^{12} ions/m^3, respectively. At the same ion flow rate, the magnitude of the number concentration for a negative ion was slightly higher than that of the positive ion, again because negative and positive ions differ in mass and electrical mobility. Ionic mobility was inversely proportional to its mass. Generally, values of mobility for positive and negative ions differ by approximately 19.30%. Reischl et al. [20] quote averages for ion motility as 1.15×10^{-4} and 1.425×10^{-4} m^2/V s for positive and negative ions.

Fig. 11 shows the space charge and diffusion precipitates of ions as a function of ion flow rate. Positive and negative ion precipitates due to space charge and diffusion effects ranged from 92 to 97 % and 91−97 % for ion flow rates in the range of 1−5 L/min. Higher ion flow rates resulted in further reducing the space charge and diffusion precipitates of ions. Figs. 12−14 show the time variations of outlet ion concentration with collection voltage at different ion flow rates. For this study the collection voltages varied from 0 to 45 V, the ion flow rates from 1 to 5 L/min and the times of measurement from 0 to 100 s. It was found in Figs. 12−14 that the concentration of positive ions was more stable than that of negative ions. This was because a negative ion had a higher electrical mobility than a positive ion due to a negative corona in the corona discharge ionizer has much higher density of free electrons compared to a positive corona, perhaps a thousandth of the electron density, and a hundredth of the total number of electrons. However, the electrons in a positive corona were concentrated close to the surface of the curved electrode in region of high potential gradient; however, the electrons in a negative corona many
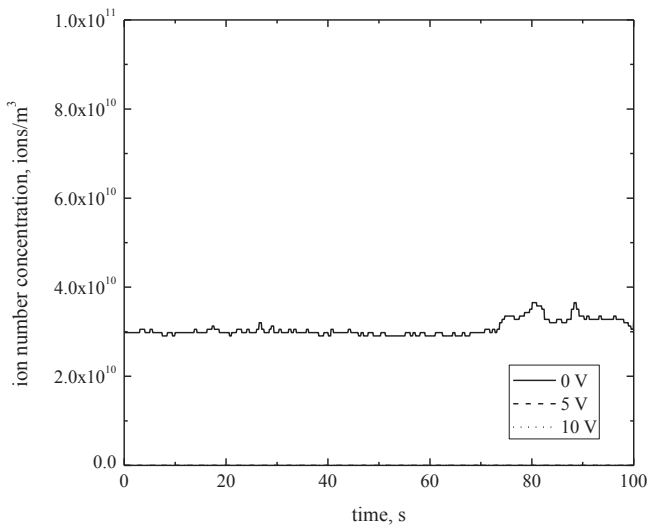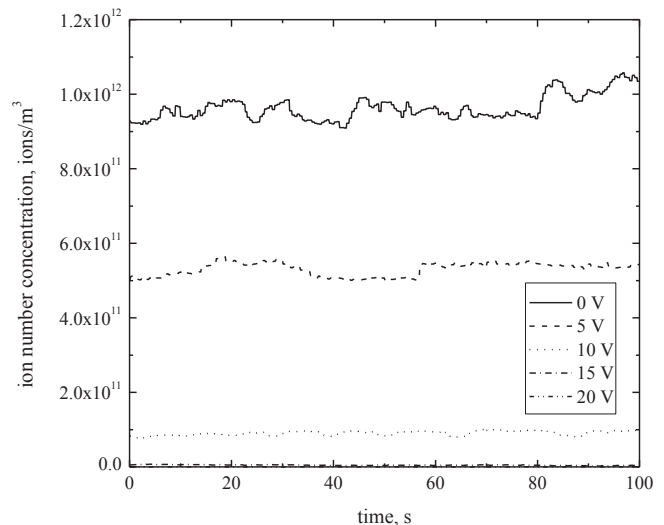

(a) positive corona
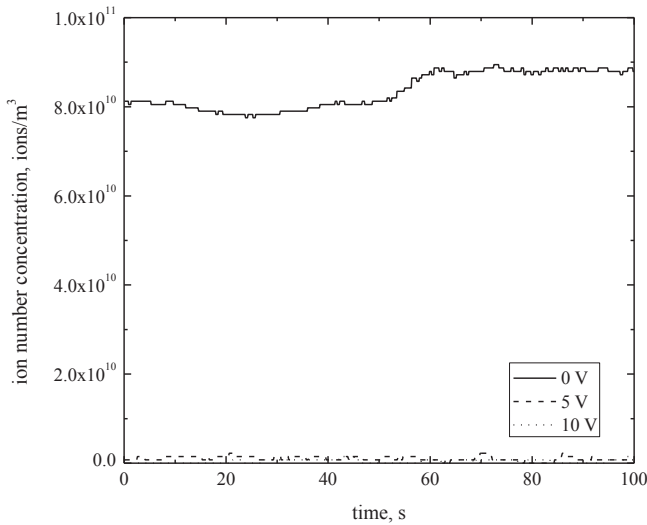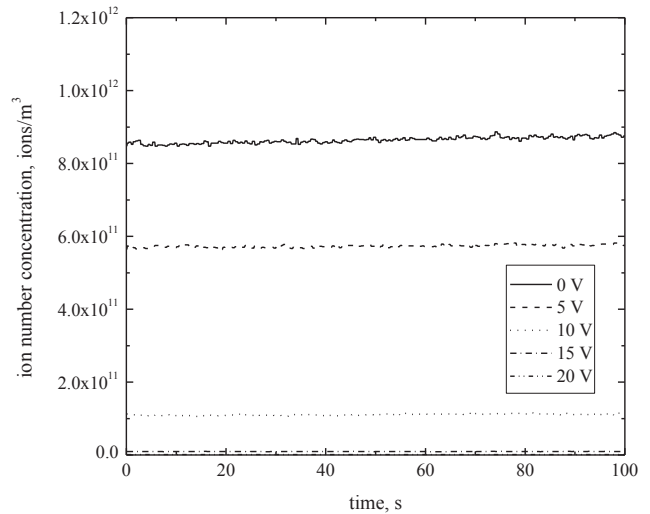
(b) negative corona

Fig. 12. Time variation of outlet ion concentration with collection voltage at ion flow rate of 1 L/min.

(a) positive corona

(b) negative corona

Fig. 13. Time variation of outlet ion concentration with collection voltage at ion flow rate of 3 L/min.

of electrons are in the outer lower-field areas [17]. Increasing the collection voltage resulted in the decrease of the ion number concentration at the collector outlet. Fig. 15 shows the variation of outlet ion concentration with collection voltage at different ion flow rates. Low ion flow rate and high collection voltage resulted in a decrease in the number concentration of ions at the collector outlet. For positive and negative ions, the ion number concentration at the collector outlet decreased to about 0 at collection voltages greater than 5, 20, and 40 V for ion flow rates of 1, 3, and 5 L/min, respectively.
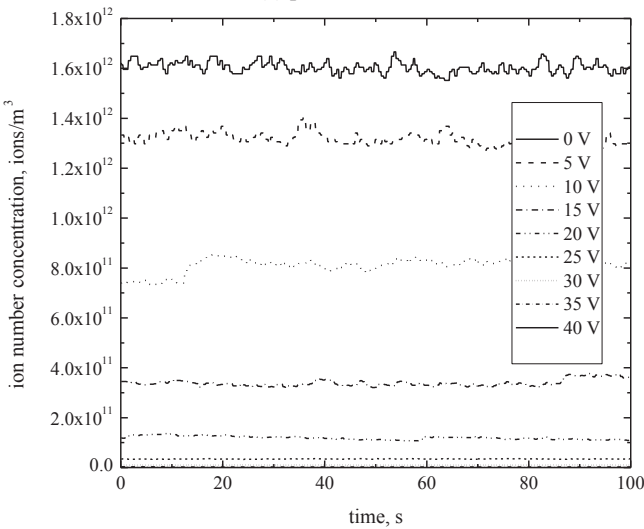
Fig. 16 shows the variation of collection efficiency with collection voltage at different ion flow rates. Generally, an increase in collection voltage produced an increase in the ion collection efficiency of the collector for both negative and positive ions. It was shown that the ion collection efficiency of the collector increased to 100% at a collection voltage larger than 5 and ion flow rate of 1 L/min, for a collection voltage larger than 20 V the ion flow rate needed to be 3 L/min and for 40 V the ion flow rate of 5 L/min also gave 100% collection. This shows that the ion collector proved to be particularly useful in collecting positive and negative ions.

Conclusion

A coaxial cylindrical collector was designed as well as numerically and experimentally studied to determine the collection efficiency of positive and negative ions. The positive and negative ions were generated by a corona-needle ionizer. For positive and negative corona voltages, the number concentration of the ions at the ionizer outlet ranged from 9.38×10^{11} to 1.91×10^{13} ions/m^3 for negative ions and 2.26×10^{12} to 1.79×10^{13} ions/m^3 for positive ions. In this study, the positively and negatively applied voltages at the inner electrode ranged from 0 to 45 V and the ion flow rates ranged from 1 to 5 L/min. For these ion flow rates (1–5 L/min), the positive and negative ion losses due to space charge and diffusion effects ranged from 92 to 97 %, and 91–97 %, respectively. Increasing the collection voltage resulted in a decrease of the ion number concentration at the collector outlet, consequently; an increase in ion collection efficiency of the collector. The total collection efficiency of positive and negative ions of the collector
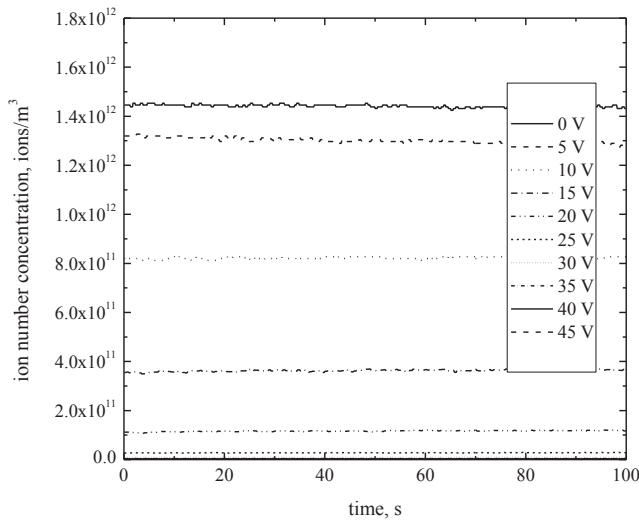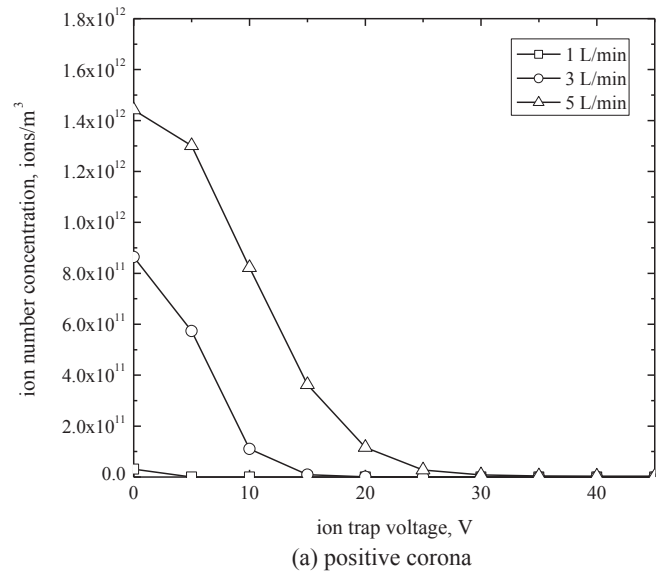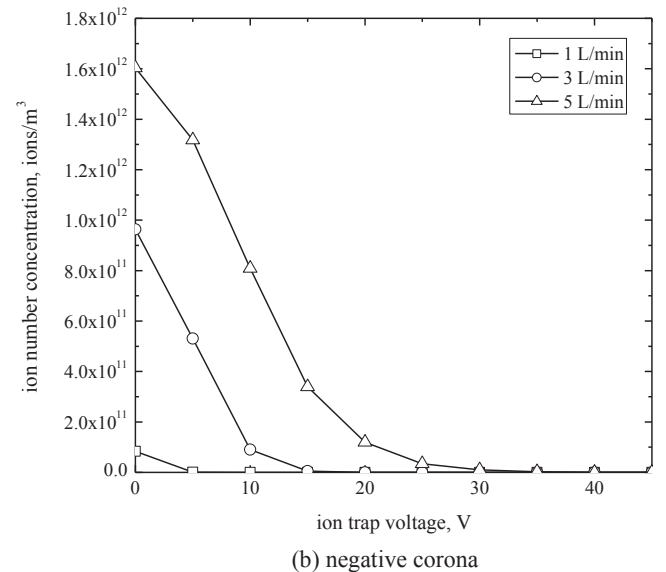

(a) positive corona

(b) negative corona

Fig. 14. Time variation of outlet ion concentration with collection voltage at ion flow rate of 5 L/min.
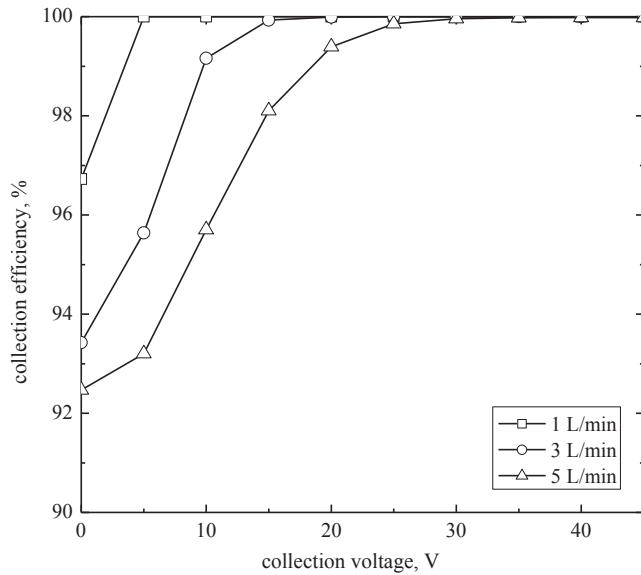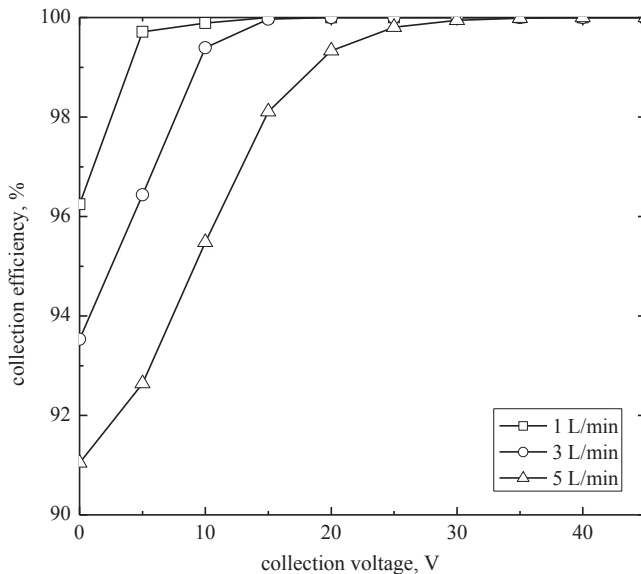

(a) positive corona

(b) negative corona

Fig. 15. Variation of outlet ion concentration with collection voltage at different ion flow rates.

(a) positive corona

(b) negative corona

Fig. 16. Variation of total collection efficiency with collection voltage at different ion flow rates.

increased to 100% at collection voltages larger than 5, 20, and 40 V for ion flow rates of 1, 3, and 5 L/min, respectively. A commercial computational fluid dynamics software package COMSOL Multiphysics™ was used to predict the behavior of the flow and electric fields as well as the particle trajectories in the collecting zone of the ion collector. Numerical simulation results of the ion trajectory in the collecting zone of the ion collector; showed good agreement with experimental results of the total collection efficiency and can be used to support the bettering of further modify and refinement of the ion collector after the charger or ionizer in a mini-volume electrical aerosol detector. These results can be used as the proper operating conditions for the ion collector. The ion collector proven to be particularly useful for collecting highly electrically mobile and positive and negative ions after the charger or ionizer of a mini-volume electrical PM detector.

Acknowledgments

References

[1] W.C. Hinds, Aerosol Technology, John Wiley & Sons, New York, USA, 1999.
[2] R.C. Flagan, History of electrical aerosol measurements, Aerosol Sci. Technol. 28 (1998) 301–380.
[3] P. Intra, N. Tippayawong, An overview of aerosol particle sensors for size distribution measurement, Maejo Int. J. Sci. Technol. 1 (2) (2007) 120–136.
[4] P. Intra, N. Tippayawong, Performance evaluation of an electrometer system for ion and aerosol charge measurements, Korean J. Chem. Eng. 28 (2) (2011) 527–530.
[5] M. Lehtimaki, Modified Electrical Aerosol Detector, Aerosol in the Mining and Industrial Work Environments, Ann Arbor Science Publishers, Ann Arbor, 1983.
[6] M. Lehtimaki, Studies of Aerosol Measuring Techniques (Ph.D. thesis), Tampere University of Technology, Tampere, Finland, 1986.
[7] J. Keskinen, K. Pietarinen, M. Lehtimaki, Electrical low pressure impactor, J. Aerosol Sci. 23 (1992) 353–360.
[8] A. Medved, F. Dorman, S.L. Kaufman, A. Pocher, A new corona-based charger for aerosol particles, J. Aerosol Sci. 31 (2000) s616–s617.
[9] TSI Incorporated, Operation and Service Manual, Revision B, for Electrical Aerosol Detector™ Spectrometer Model 3070, 2004. Minnesota, USA.
[10] J. Wei, Development of a Method for Measuring Surface Area Concentration of Ultrafine Particles (D.Eng. thesis), University of Duisburg-Essen, Germany, 2007.
[11] D. Park, M. An, J. Hwang, Development and performance test of a unipolar diffusion charger for real-time measurements of submicron aerosol particles having a log-normal size distribution, J. Aerosol Sci. 38 (2007) 420–430.
[12] P. Intra, N. Tippayawong, Use of electrostatic precipitation for excess ion trapping in an electrical aerosol detector, J. Electrost. 69 (2011) 320–327.
[13] COMSOL Inc, COMSOL Multi Physics Modelling Guide, Version 3.5a, 2008.
[14] P. Intra, N. Tippayawong, Effect of needle cone angle and air flow rate on electrostatic discharge characteristics of a corona-needle ionizer, J. Electrost. 68 (2010) 254–260.
[15] P. Intra, N. Tippayawong, Design and evaluation of a high concentration, high penetration unipolar corona ionizer for electrostatic discharge and aerosol charging, J. Electr. Eng. Technol. 8 (5) (2013) 1175–1181.
[16] P. Intra, N. Tippayawong, Measurements of ion current from a corona-needle charger using a faraday cup electrometer, Chiang Mai J. Sci. 36 (1) (2009) 110–119.
[17] E.A. Mason, Ion mobility: its role in plasma chromatography, in: T.W. Carr (Ed.), Plasma Chromatography, Plenum Press, New York, USA, 1984.
[18] H.J. White, Industrial Electrostatic Precipitation, Addison-Wesley Pub Co. U S A, 1963.
[19] B.Y.H. Liu, A. Kapadia, Combined field and diffusion charging of aerosol particles in the continuum regime, J. Aerosol Sci. 9 (1978) 227–242.
[20] G.P. Reischl, J.M. Makela, R. Harch, J. Necid, Bipolar charging of ultrafine particles in the size range below 10 nm, J. Aerosol Sci. 27 (6) (1996) 931–939.